Approaches for reduction of the temperature bias on radon detectors packed in anti-thoron polymer membranes

Krasimir Mitev, S. Georgiev, Benoit Sabot

Approaches for reduction of the temperature bias on radon detectors packed in anti-thoron polymer membranes

K. Mitev[a], S. Georgiev[a,*], B. Sabot[b]

[a] *Faculty of Physics, Sofia University "St Kliment Ohridski", 1164 Sofia, Bulgaria*
[b] *Université Paris-Saclay, CEA, LIST, Laboratoire National Henri Becquerel (LNE-LNHB), F-91120, Palaiseau, France*

Abstract

Passive and active detectors used for radon (^{222}Rn) measurements can be influenced by thoron (^{220}Rn). Polyethylene membranes are very appropriate diffusion barriers for anti-thoron protection of such detectors. However, if not properly chosen, these membranes may not reduce efficiently the thoron influence or could introduce temperature bias in the radon sensitivity of the detectors. In this work three approaches are proposed dealing with the thoron influence reduction and the temperature bias introduced by packing in polymer membranes: An approach that allows to optimize the membrane properties to efficiently reduce the thoron influence while introducing small temperature bias; A differential approach that uses two passive devices packed in membranes of different diffusion properties, that allows to perform good thoron suppression and to estimate and correct for the temperature bias in ^{222}Rn readings; And an approach for temperature correction applicable for monitors with anti-thoron membrane that uses the temperature data of the monitor to correct for the temperature bias.

Keywords: Radon, Thoron, Radon detectors, Polymer membranes, Temperature bias, Thoron influence

*Corresponding author
Email address: strahilg@phys.uni-sofia.com (S. Georgiev)

1. Introduction

Radon (^{222}Rn, half-life $T_{1/2}$=3.8232(8) d (Bé et al., 2016)) is widely spread near the earth surface, as it is a part of the natural radioactive chain of ^{238}U. As an inert gas with a relatively long half-life, radon could migrate far from the spot of its generation and could accumulate indoors. The indoor radon is responsible for more than 50% of the annual effective dose of the general population from natural sources (UNSCEAR, 2000) and is the leading cause for lung cancer for non-smokers (WHO, 2009). Thoron (^{220}Rn, $T_{1/2}$=55.8(3) s (Bé et al., 2016)) is also a part of a natural radioactive chain (^{232}Th series) and could also be a health hazard (UNSCEAR, 2000; Tokonami et al., 2001; UNSCEAR, 2008; Chen and Moir, 2012). However, due to its much shorter half-life, it could only migrate a short distance. Therefore, thoron reaches hazardous concentrations indoors only at specific conditions (Tokonami et al., 2001; UNSCEAR, 2008; Meisenberg et al., 2017).

Dealing with the indoor radon is a complex task with several aspects: identifying buildings with high radon, finding/locating the sources of radon, performing risk assessment, mitigation, etc. To address these, various methods were developed, which use passive devices or monitors with passive and/or active sampling (Ward III et al., 1977; Fleischer et al., 1980; Tommasino, 1990, 1998; Nikolaev and Ilić, 1999; Papastefanou, 2002; Mark Baskaran, 2016; Galli et al., 2019). The passive devices, such as diffusion chambers with Solid-State Nuclear Track Detector (SSNTD) or electret detector or charcoal canisters, use passive detectors and passive radon sampling. The monitors use active detectors such as PIPS-detectors, Lucas cell, ionization chambers, etc. and passive or active sampling (e.g. passive diffusion through a diffusion barrier or active air-sampling with a pump).

Most radon detectors employ the secular equilibrium between radon and its Short-lived Decay Products (SDPs) in the detector's volume and measure radon by detecting the alpha-particles of radon (^{222}Rn) and its SDPs – ^{218}Po and ^{214}Po. Thoron has similar decay scheme with several short-lived alpha-

emitters – ^{220}Rn, ^{216}Po, ^{212}Bi and ^{212}Po. That makes all these radon detectors (passive devices and monitors) potentially sensitive to both radon and thoron (Ward III et al., 1977; Fleischer et al., 1980; Tommasino, 1990, 1998; Nikolaev and Ilić, 1999; Ggriffith and Tommasino, 1990; Michielsen and Bondiguel, 2015; Dwivedi et al., 2001; Bochicchio et al., 2009). There are three commonly used approaches to discriminate between radon and thoron:

The *alpha-spectrometry* is probably the best way to discriminate between radon and thoron. For example, the semiconductor detectors allow good enough energy resolution to discriminate between the alpha-peaks of radon, thoron and their SDPs. However, this approach is applicable only to monitors.

The idea of the *"delayed-measurements"* is to delay the measurement of the sampled air for a few minutes and let thoron ($T_{1/2}$=55.8(3) s (Bé et al., 2016)) and ^{216}Po ($T_{1/2}$=0.148(4) s (Bé et al., 2016)) decay. The other two alpha-emitters among the thoron's SDPs are preceded by ^{212}Pb, which has a long enough half-life of 10.64(1) h (Bé et al., 2016), so that they would not contribute to the signal in a short-term radon measurement. Similar concept is used in AlphaGUARD PQ2000 PRO (Rn/Tn) to measure radon and thoron simultaneously. The sampled air is pumped for a few minutes in the pulsed ionization chamber of the detector and is measured during the pumping, then the pumping is stopped and the air is measured again. These two measurements are used to estimate both radon and thoron. For long-term measurements the thoron concentration estimated in previous intervals is used to calculate the build-up of ^{212}Pb and the two alpha-emitters that follow after it and to correct for their influence. This approach is more complicated and is applicable only when active sampling is used.

The *diffusion barriers* such as polymer membranes, spongy materials or thin air-gaps are used in almost all passive devices and monitors with passive sampling. Their purpose is to keep out the SDPs present in the ambient air and to let radon enter inside the detector's volume (Ward III et al., 1977; Fleischer et al., 1980; Tommasino, 1990, 1998; Nikolaev and Ilić, 1999; Ggriffith and Tommasino, 1990; Dwivedi et al., 2001; Bochicchio et al., 2009).

As the SDPs are attached to dust particles or grouped in clusters, they are stopped by the diffusion barrier, while the inert-gas atoms could diffuse through it. Additionally, as the thoron atoms decay much faster, their diffusion length (mean path traveled by the atoms before decay) in the diffusion barrier is much shorter than the diffusion length of radon atoms. Thus, if the barrier thickness and diffusion properties are carefully chosen, it could reduce significantly the thoron penetration through it, while it remains almost transparent to radon (Ward III et al., 1977; Fleischer et al., 1980; Tommasino, 1990, 1998; Ggriffith and Tommasino, 1990; Dwivedi et al., 2001; Bochicchio et al., 2009; Hafez and Somogyi, 1986; Miles et al., 2009). However, the diffusion properties of the diffusion barriers are temperature dependent and that could lead to two types of bias: 1. A thoron influence: With the increase of the temperature, the diffusion length also increases and the barrier could become partially transparent to thoron and at high temperature could introduce non-negligible, temperature-dependent thoron contribution to the radon measurement; 2. A temperature bias of the radon response: The temperature variations also influence the radon diffusion length which could change the transparency of the barrier to radon and thus to bias the radon signal of the detector (Tommasino, 1990, 1998; Ggriffith and Tommasino, 1990; Fleischer et al., 2000).

Although the air-gaps and the spongy materials are successfully used as diffusion barriers in some detectors, the polyethylene (PE) membranes are probably the best choice, because their diffusion properties allow good radon/thoron discrimination at common indoor and outdoor temperatures. Therefore, the purpose of this work is to address the thoron influence and the temperature bias introduced by the diffusion barrier, considering PE membranes.

For that purpose a previously proposed model (Mosley, 1996) is adopted, modified and further developed to describe the transport of radon and thoron from the ambient media to the volume of the detector through a PE membrane with known diffusion properties. The modified model is experimentally validated. Based on that model three approaches for dealing with the thoron influence and the temperature bias are proposed. Additionally, a novel device

used in the presented studies is shown to be very appropriate for estimation of the permeability of membranes.

2. Theoretical modeling

Radon detectors, such as passive devices and monitors with passive sampling, consist of a passive or active detector for alpha-particles (in most of the cases), placed in a well-defined volume isolated from the ambient air by a diffusion barrier. The polymer barriers, particularly the low density polyethylene (LDPE) membranes, seem to be very appropriate choice for a diffusion barrier due to several advantages that they offer:

- The temperature dependence of their diffusion properties could be estimated precisely and the radon transport through them could be modeled (Mosley, 1996; Georgiev et al., 2019);
- They are hydrophobic – their diffusion properties are not influenced by the humidity and they ensure water resistance for the detectors (Tommasino, 1990, 1998; Ggriffith and Tommasino, 1990; Miles et al., 2009; Azimi-Garakami et al., 1988) (some detectors are sensitive to humidity/moisture (Hopper et al., 1999; De Simone et al., 2016));
- They are airtight. If the detector volume is not airtight, that could lead to active transport through the diffusion barrier and cause change of the thoron influence and the radon sensitivity of the detector;
- The LDPE foils are durable, flexible and they are produced in various thicknesses, so their radon/thoron diffusion properties could be precisely chosen and they could be easily manipulated to fit almost everywhere;
- Because of the above mentioned mechanical properties, they could be applied to already existing detectors with other types of diffusion barriers.

Therefore, in the present work LDPE membranes are considered, however the model could be easily applied to other types of diffusion barriers.

2.1. Diffusion model

In (Mosley, 1996) a method for measuring the diffusion coefficient D of radon in thin films is presented. The experimental setup is shown in Figure 1. It consist of two chambers separated by the studied film and an alpha-detector inside the accumulation chamber (detector's volume). To study the diffusion coefficient, a model of radon transport through the membrane and the build-up of radon in the accumulation chamber is developed. It is considered that the diffusion of radon through the thin film is described by one-dimensional diffusion equation with additional term that accounts for the radioactive decay:

$$\frac{\partial c}{\partial t} = D\frac{\partial^2 c}{\partial x^2} - \lambda c, \tag{1}$$

where $c = c(x,t)$ is the radon atomic concentration inside the film, λ is the decay constant of radon, t is a time variable and x is a space coordinate in direction perpendicular to the surface of the film. It is also stated that steady state diffusion in the thin film is reached for a characteristic time (Mosley, 1996):

$$\tau_r = \frac{1}{\lambda + \frac{\pi^2 D}{d^2}} = \frac{1}{\lambda\left(1 + \left(\frac{\pi L_D}{d}\right)^2\right)}, \tag{2}$$

where d is the thickness of the film and $L_D = (D/\lambda)^{1/2}$ is the diffusion length of radon in the film's material. If that characteristic time[1] is much smaller than the life-time of radon $\tau_r << 1/\lambda$ or equivalently $d << \pi L_D$ (see Eq. 2), it could be assumed that the transport of radon through the film is at steady-state condition (Mosley, 1996), which leads to $\partial c/\partial t = 0$. On the other hand, the higher the ratio L_D/d is, the more permeable the film is and as the film should be permeable to radon, the steady-state condition should be satisfied. In that case, Eq. 1 is solved with boundary conditions $c(x = 0) = C_{out}$ and

[1]For instance, for membranes made of LDPE ($L_D \approx$1 mm (Georgiev et al., 2019)) and of polycarbonate (PC) ($L_D \approx$0.05 mm (Georgiev et al., 2019)) with thickness $d \approx$0.1 mm, these times are $\tau_{r,LDPE} \approx 8$ min and $\tau_{r,PC} \approx 40$ h.

$c(x = d) = C_{in}$:

$$c(x) = \frac{C_{out} \sinh\left((d - x)/L_D\right) + C_{in} \sinh\left(x/L_D\right)}{\sinh\left(d/L_D\right)}, \tag{3}$$

where C_{out} is the radon concentrations in the ambient media (the source chamber) and C_{in} is that in the accumulation (detector's) volume. At this point, the first modification to the model described in [3] is made, because this model does not take into account the partition coefficient of radon between the air and the polymer. In this work the partition coefficient $K = C_P/C_M$ is defined as the ratio of the concentration at the two sides of the border between the polymer (C_P) and the ambient media (C_M) and K depends on the temperature. Another modification is introduced to account for exponentially decreasing radon concentration in the source chamber opposed to the constant radon concentration used in (Mosley, 1996): Prompt introduction of radon in the exposure system at the beginning of the experiment, followed by radon decrease during the experiment due to radioactive decay and leakage (if the source chamber is not fully hermetic to ^{222}Rn) described as $C_{out} = C_{0,out} e^{-\lambda_{out} t}$, where λ_{out} accounts for both leakage and radioactive decay. If the leakage is small ($\tau_r << 1/\lambda_{out}$), then Eq. 3 is modified to:

$$c(x) = K \frac{C_{0,out} \sinh\left((d - x)/L_D\right) e^{-\lambda_{out} t} + C_{in} \sinh\left(x/L_D\right)}{\sinh\left(d/L_D\right)}. \tag{4}$$

Including the partition coefficient in the model is important as the partition coefficient of radon in some polymers could be much greater than 1. This would increase significantly the radon concentration inside the membrane which would enhance the radon transport through it. If λ_{out} is set to zero (i.e. no decrease in the radon concentration), then $C_{out}(t) = constant$ and Eq. 4 takes the form of the corresponding equation obtained by the original model (Mosley, 1996).

In the model of Mosley (1996), the build-up rate of radon in the detector's volume is described as a build-up due to radon inflow through the membrane and radon loss due to radioactive decay:

$$\frac{dC_{in}(t)}{dt} = J_c(t, x = d)\frac{S}{V} - \lambda C_{in}(t)$$
$$= -D\frac{S}{V}\frac{\partial c(t,x)}{\partial x} \mid_{x=d} -\lambda C_{in}(t), \tag{5}$$

where $J_c(t, x = d) = -D(\partial c/\partial x) \mid_{x=d}$ is the radon flux through the membrane at the detector's side. Considering $c(x)$ given by Eq. 4, the radon flux is calculated:

$$J_c(t, x = d) = -D\frac{\partial c(t,x)}{\partial x} \mid_{x=d} = \frac{P}{L_D}\frac{C_{0,out}e^{-\lambda_{out}t} - C_{in}\cosh(d/L_D)}{\sinh(d/L_D)}, \tag{6}$$

where the quantity $P = KD$ is the permeability of radon through the membrane. Combining Eqs 5 and 6 leads to:

$$\frac{dC_{in}(t)}{dt} + \big(\lambda + \frac{PS}{VL_D\tanh(d/L_D)}\big)C_{in}(t) = \frac{PS}{VL_D\sinh(d/L_D)}C_{0,out}e^{-\lambda_{out}t}. \tag{7}$$

Considering an initial condition $C_{in}(t = 0) = 0$, the solution of Eq. 7 is:

$$C_{in}(t) = \frac{C_{0,out}e^{-\lambda_{out}t}}{(1 + \frac{\lambda}{\lambda_d})\cosh(d/L_D)}\big(1 - e^{(-(\lambda+\lambda_d)t)}\big) \tag{8a}$$

$$C_{in}(t >> \tau_{eq}) = \frac{C_{0,out}e^{-\lambda_{out}t}}{(1 + \frac{\lambda}{\lambda_d})\cosh(d/L_D)} \tag{8b}$$

where $\tau_{eq} = (\lambda + \lambda_d)^{-1}$ is the characteristic time for reaching equilibrium radon concentration in the detectors volume and λ_d accounts for radon transport through the membrane:

$$\lambda_d = \frac{PS}{VL_D\tanh(d/L_D)}. \tag{9}$$

It should be noted that solving the partial differential equation (7) yields to the solution (8) with a term ($C_{0,out}e^{-\lambda_{out}t}$) which is the same as the inhomogeneous (right-hand side) part of (7) and actually represents the time dependence of the outside (source) concentration. It is also seen from Eq. 8b that after certain period of time $t >> \tau_{eq}$ the inner radon activity concentration is proportional

to the outside activity concentration $C_{in}(t) \propto C_{out}(t)$. Additionally, as the membrane should be permeable to radon, then the condition $L_D >> d$ should be fulfilled. Taking into account that $\cosh(d/L_D) \to 1$ and $\tanh(d/L_D) \to d/L_D$ when $(d/L_D) \to 0$, the Eqs. 8 and 9 could be simplified to:

$$C_{in}(t) = \frac{C_{out}(t)}{(1 + \frac{\lambda}{\lambda_d})}\left(1 - e^{(-(\lambda+\lambda_d)t)}\right) \tag{10a}$$

$$C_{in}(t >> \tau_{eq}) = \frac{C_{out}(t)}{(1 + \frac{\lambda}{\lambda_d})} \tag{10b}$$

with:

$$\lambda_d = \frac{PS}{Vd}, \tag{11}$$

If equilibrium is reached much faster than the change in the outside activity concentration, then the inner concentration C_{in} will follow the outer concentration C_{out} and the ratio $R = C_{in}/C_{out}$ should be constant at the given temperature and should only depend on λ_d. Thus, if the ratio R is estimated (e.g. experimentally) then the permeability could be determined, or, if the permeability of the membrane is known, then the bias in the response of the detector could be predicted and its readings could be corrected, which is the basic idea in the current manuscript.

It is also of interest to consider the model with an initial activity concentration inside the detector's volume $C_{in}(t = 0) = C_{0,in}$ and a zero concentration outside $C_{out}(t) = 0$ – e.g. a packed passive device exposed to radon and then left to degas in radon-free air. The changes in the model that these conditions yield, lead just to setting $C_{0,out} = 0$ in Eqs 4, 6 and 7. Thus, Eq. 7 becomes homogeneous and its solution is:

$$C_{in}(t) = C_{0,in}e^{(-(\lambda+\lambda_d)t)} \tag{12}$$

In the case of passive device exposed for time t_{exp} the activity concentration $C_{0,in}$ in the device volume at the end of the exposure could be obtained, if the

time t in Eq. 10 is set to t_{exp}. Thus, Eq. 12 takes the form:

$$C_{in}(t_d) = \Big[\frac{C_{out}(t)}{(1+\frac{\lambda}{\lambda_d})}\big(1-e^{-(\lambda+\lambda_d)t_{exp}}\big)\Big]e^{-(\lambda+\lambda_d)t_d} \tag{13}$$

where t_d is the degassing time and the initial moment $t_d = 0$ is at the end the exposure. It could be shown by Fleischer et al. (1980) that for a passive device exposed in a packing, if it is left to degas in its packing for time $t_d >> (\lambda+\lambda_d)^{-1}$, its signal is proportional to the average ambient activity concentration during the exposure:

$$n_0 = CF\frac{\overline{C}_{out}t_{exp}}{1+\frac{\lambda}{\lambda_d}} = CF\frac{\overline{C}_{out}t_{exp}}{1+\lambda\frac{Vd}{PS}} \tag{14}$$

where n_0 is the net signal of the passive device (e.g. the net track density of a SSNTD) and CF is the calibration factor of the device.

Application of the diffusion model to thoron

Due to the relatively short half-life of thoron, all transitional processes (diffusion through the membrane and build-up in the detector's volume) terminate within less than 10 minutes. This time is much shorter than the typical times of practical interest, e.g. calibration exposures, field measurements with passive detectors or dynamics follow up with monitors. Therefore, in the case of thoron Eq. 1 is considered with steady-state condition $\partial c/\partial t = 0$. Actually, this yields the same solutions for the thoron distribution $c(x)$ in the diffusion barrier (membrane) given by Eq. 4 and for the thoron flux $J_c(t, x = d) = -D(\partial c/\partial x)\mid_{x=d}$ through the membrane at the detector's side given by Eq. 6. Then, Eq. 5 is also considered with steady-state condition $dC_{in}(t)/dt = 0$ and solution for the flux given by Eq. 6 is substituted in it. This leads to a linear (not differential) equation with solution:

$$C_{in,Tn}(t) = \frac{C_{out,Tn}(t)}{(1+\frac{\lambda_{Tn}}{\lambda_{d,Tn}})\cosh\left(d/L_{D,Tn}\right)}, \tag{15}$$

and

$$\lambda_{d,Tn} = \frac{PS}{VL_{D,Tn}\tanh\left(d/L_{D,Tn}\right)}, \tag{16}$$

where $C_{in,Tn}(t)$ and $C_{out,Tn}(t)$ are the thoron concentrations in the detector's volume and the ambient media, λ_{Tn} is the thoron decay constant and $L_{D,Tn} = (D/\lambda_{Tn})^{1/2}$ is the diffusion length of thoron in the membrane's material. Equations 15 and 16 are very similar to those for radon (see Eqs 8b and 9): the permeability of the membrane $P = KD$ is considered the same for radon and thoron as their atoms are chemically the same and, essentially, the differences are due to the different decay constants of radon and thoron. Following from the definition the diffusion lengths of radon and thoron are related as: $L_D/L_{D,Tn} = (\lambda_{Tn}/\lambda)^{1/2}$.

2.2. Application of the diffusion model to passive devices

In the present work two approaches based on the diffusion model are proposed that account for the thoron and the temperature influence on the radon signal of passive devices packed in a polymer foil.

The **optimization approach** allows an estimation of the effect of a given packaging and an optimization of the parameters of the packaging in order to minimize the thoron and the temperature influence. An example for such an optimization is shown in Figure 2 considering a LDPE membrane with known diffusion properties (Georgiev et al., 2019). It is also considered that the passive device is calibrated in the packaging at temperature T=20°C and during the field measurements the temperature variations are in the interval 10-30°C (which is an overestimated interval of the typical indoor temperature variations). In Figure 2 the thoron influence is shown as the part of the ambient thoron activity concentration that penetrates the packed volume: $R_{Tn} = C_{in,Tn}/C_{out,Tn}$, estimated by Eq. 15. The temperature influence on the radon signal is shown as the relative difference $R_{in} = \frac{(C_{in}(T) - C_{in}(20°C))}{C_{in}(20°C)}$, where $C_{in}(T)$ and $C_{in}(20°C)$ are estimated by Eq. 10b assuming the same ambient activity concentration

for both temperatures. Because both $P(T)$ and $L_D(T)$ increase with the temperature, the temperature bias is positive at higher temperatures (compared to the temperature during the calibration) and negative at lower temperatures (Fig. 2). Thus, this is an estimation of the maximum bias – if the temperature is systematically either lower or higher than the temperature during the calibration. In the case of random variation, this bias should be smaller. The thoron and the temperature influence are given as functions of (Vd/S) and once the V/S ratio is known the optimum value of d could be chosen (see Eqs 11 and 16). The range of the (Vd/S)-axis in Figure 2 is chosen so it could match real detectors' dimensions and reasonable LDPE membrane thicknesses. It is seen that if, for example, (Vd/S)=0.001 cm^2, then the maximum thoron influence could be less than 2% and the maximum temperature influence could also be about 2%. The optimization approach would in many cases allow a reasonable reduction of the thoron influence without introducing a significant temperature bias. The temperature bias could be estimated and added to the uncertainty budget of the measurement.

The differential method (the second approach) allows to estimate the temperature influence and to correct the signal of the passive device. It requires two passive devices to be used in the radon measurement. These two devices, called a "device couple", should be packed in packages with different diffusion properties. The most simple way to do that is to use the same geometry (V/S) and the same material (P and L_D) of the packings with difference only in the membrane thicknesses. The idea of this approach is to use the ratio $R_s = n_1/n_2$ of net signals n_1 and n_2 of the two devices in the couple and the temperature dependence of this ratio $R_s(T)$ in order to estimate the temperature and then to correct the signal of the device couple.

This could be done by using identical devices for the device couple calibrated at a single temperature. As the devices are identical, they should have one and the same sensitivity (or calibration factor CF) to radon. Thus, using Eq. 14

the signal ratio could be expressed as:

$$R_s(d_1, d_2; T) = \frac{n_1}{n_2} = \frac{1 + \frac{\lambda}{\lambda_{d,2}}}{1 + \frac{\lambda}{\lambda_{d,1}}} = \frac{1 + \lambda \frac{Vd_2}{SP(T)}}{1 + \lambda \frac{Vd_1}{SP(T)}}, \tag{17}$$

The rational function $R_s(P)$ is monotonous and it increases with the increase of P if $d_1 < d_2$ or it decreases with the increase of P if $d_1 > d_2$. It could be solved in respect to the permeability:

$$P = \frac{\lambda V}{S} \frac{d_2 - d_1 R_s}{R_s - 1}. \tag{18}$$

This allows the device couple to be used to estimate the permeability of the membrane. On the other hand, as the temperature dependence of the permeability is already known, it could be used to estimate the exposure temperature. Further, if the devices are calibrated with no packaging (bare), the correction coefficient κ to be applied to the calibration factor of a packed device is given by the ratio of the activity concentrations inside and outside the packaging: $\kappa = C_{in}/C_{out}$ and could be estimated by the diffusion model (Eq. 10b). The permeability from Eq. 18 could be substituted in Eq. 10b to obtain a direct relation $\kappa(R_s)$:

$$\kappa_1 = \frac{1}{1 + \lambda \frac{Vd_1}{SP}} = \frac{d_2 - R_s d_1}{d_2 - d_1} \tag{19a}$$

$$\kappa_2 = \frac{1}{1 + \lambda \frac{Vd_2}{SP}} = \frac{d_2 - R_s d_1}{R_s(d_2 - d_1)}. \tag{19b}$$

Then, the experimental value of $R_s = n_1/n_2$ could be used to estimate the correction coefficients κ_i (Eq. 19) and to correct the calibration factors of both devices $CF_i = \kappa_i CF$.

The differential method could also be applied without using the theoretical model to estimate the correction. This is a great advantage if the two devices in the couple are different or if the permeabilities of the packings are different: It is required that the devices in the couple are calibrated (in their packings) at several different temperatures, in order to obtain the functions $R_s(T)$ and

$CF_i(T)$, where CF_i are the calibration factors of the packed devices. Then, in the field radon measurement, the ratio $R_s = n_1/n_2$ could be estimated by the device couple signals and the already known function $R_s(T)$ to be used to deduce the exposure temperature and through it the calibration factors $CF_i = CF_i(T)$. Moreover, the device couple could be calibrated directly versus the R_s-ratio – $CF_i(R_s)$ and then the experimentally estimated $R_s = n_1/n_2$ to be used to estimate directly $CF_i = CF_i(R_s)$ without the intermediate estimation of the temperature.

The diffusion model allows some general considerations to be drawn that should be followed with both the optimization approach and the differential method:

- The ratios R_s and C_{in}/C_{out} depend on the S/V-ratio of the packaging. The higher the S/V-ratio is, the smaller the temperature bias (C_{in}/C_{out}) and the temperature sensitivity of R_s are. Varying the S/V-ratio allows modification of the temperature sensitivity of the device couple;
- The temperature sensitivity of R_s could be increased if the packings of the two devices differ significantly in their thicknesses d_1 and d_2;
- One of the devices should be packed with a membrane with a small thickness, so that the temperature correction would be small (i.e. κ to be close to 1);
- If the packaging is very thick (so that λ_d becomes comparable to or smaller than λ), it could introduce a significant decrease of the radon sensitivity of the packed detector.

2.3. Application of the diffusion model to a monitor with passive sampling

The radon monitors with passive sampling already have diffusion barriers (incl. polymer membranes) that aim to prevent the diffusion of radon SDPs from the ambient media in the detector's volume. These barriers also impede the thoron diffusion in the monitor at different level. The diffusion model allows to choose suitable polymer membrane as an anti-thoron barrier in order

to reduce the thoron influence under a desired level. Nevertheless, the membrane (or any other diffusion barrier) will introduce temperature dependence of the readings of the monitor as the diffusion properties of the materials are temperature dependent. Currently, most of the radon monitors have an in-built temperature sensor. The idea of this approach is to use the temperature data from the monitor, the known temperature dependence of the permeability $P(T)$ of the membrane and the diffusion model (Eq. 10) to perform correction of the monitor's measurement. As noted, the diffusion barriers slow down the diffusion of thoron in the monitor's volume in order to reduce its influence. Inevitably this also slows down the diffusion of radon and introduces a delay in the response of the monitor. Therefore, this approach is not suitable for devices that need fast response (e.g. devices that are supposed to follow fast changes in the radon concentration).

3. Experimental

The experimental setup used in this work is shown in Figure 3. It consists of two parts. The "Exposure setup" (the left part in Figure 3) used to create radon/thoron atmosphere and to perform exposure at different temperatures, is described in details by Pressyanov et al. (2017). It consists of a 50 L hermetic vessel (50.4 L Emanation Calibration Container, Saphymo GmbH, Germany), peristaltic pump with variable flow-rate, radon/thoron monitor AlphaGuard PQ2000 RnTn Pro with AlphaPump (Saphymo GmbH, Germany), a certified flow-through thoron source (Pylon Electronics Inc., Canada), a certified flow-through radon source (Czech Metrological Institute, Czech Republic), a specially designed thermostat (the 50 L vessel could fit in it) capable to sustain constant temperature or to reproduce predefined temperature variations in the temperature interval [-10°C;+60°C], additional accessories such as: valves, connecting hoses, filters, smaller glass vessel with volumes from 0.2 L to 10 L.

The other part of the experimental setup is the "PIPS-system" (the right part in Figure 3). It is a modified version of the French reference thoron detector

developed at Laboratoire National Henri Becquerel (CEA/LNHB). This primary thoron detector is described in detail in (Sabot, 2015; Sabot et al., 2016). The PIPS-system is based on a PIPS-detector coupled to an electric field in order to catch the decay products of radon or thoron at the surface of the detector. To allow the precise study (including the dynamics) of the transport of radon and thoron through polymer membranes in a well-defined volume, the primary thoron detector (Sabot, 2015; Sabot et al., 2016) was modified and now it possesses two chambers as shown in Figure 3: The lower chamber with circulation of air containing radon and/or thoron; and the upper chamber, which is separated by a stainless steel grid and has metalized surface in front of the silicon detector, in order to perform direct measurement of the gas and the decay products. The grid between the two chambers allows any kind of thin membrane to be placed and then to perform measurement of the radon and/or thoron passing through the membrane. The PIPS-detector was connected to real-time digital pulse processor and digital multichannel analyzer nanoMCA (labZY, USA) in order to acquire and analyze the the energy spectra of the alpha-particles.

In the present work two series of experiments were conducted. The first series was dedicated to the validation of the diffusion model and to the proof of concept of the differential method. For that purpose metallic diffusion chambers with Kodak-Pathe LR115/II SSNTDs were used. These diffusion chambers are cylindrical metallic cans with radius r=3.5 cm and height h=8 cm. The cans have metallic caps and the SSNTDs are stuck on the inner surface of the caps. The cups close tight enough to ensure hermeticity of the cans for SDPs of radon and thoron. Diffusion chambers of this type were packed in LDPE foils of different thicknesses with known diffusion properties[2] (Georgiev et al., 2019) and exposed in air with known radon concentration at three different temperatures.

[2]Among the LDPE foils used in the current work, the diffusion properties of only the "100 μm"-foil were studied in (Georgiev et al., 2019). All foils are from the same supplier's batch and the other two foils ("18 μm" and "40 μm") are considered to have the same diffusion properties.

The thicknesses of the foils declared by the supplier were approximately 18 μm, 40 μm and 100 μm, but the exact thicknesses of the foils were measured by a micrometer with a resolution of 1 μm. The differences of the measured and the declared thicknesses were within 10%. In each exposure eight chambers were exposed – a couple of bare (not packed) chambers and the rest six – packed individually, each two in a foil of a given thickness. For all the experiments, the LDPE foils of each thickness were cut from a single bigger sheet (incl. the second series of experiments, described further in the manuscript). The exposures were carried out with the exposure setup shown in Figure 3 with the PIPS-system excluded. During the exposures, the pump flow-rate was constant in order to ensure constant activity concentration in the 50 L vessel with the diffusion chambers placed in it. The activity concentration and the temperature were monitored during the exposure by the AlphaGUARD. After the exposure, the chambers have been left at the same temperature in radon-free air for time sufficient for them to degas. The exposure conditions are summarized in Table 1.

Table 1: Exposure conditions in the experiments with diffusion chambers packed in LDPE foils of different thicknesses or exposed "bare". The time-integrated radon activity concentration is estimated as $I_C = \overline{C}_{out} t_{exp}$. The permeability of the LDPE foil is estimated from the dependence $P(T)$ in (Georgiev et al., 2019). The measured average thickness of the foils is given with indexes "18", "40" and "100" corresponding to the thicknesses in [μm] declared by the supplier. The average surface and the average volume of the packings are also given. All the uncertainties are at the level of 1σ.

T[°C]	$\overline{C}_{out}$ [kBq/m^3]	t_{exp}[h]	I_C [kBq h/m^3]	P [10^{-13} m^2/s]
10(1)	19.7(15)	335.7	6600(500)	48(10)
20(1)	19.4(14)	264.0	5120(370)	108(22)
30(1)	18.4(14)	167.7	3080(240)	244(49)
$\overline{d}_{18}$ [μm]	$\overline{d}_{40}$ [μm]	$\overline{d}_{100}$ [μm]	$\overline{S}$ [cm^2]	$\overline{V}$ [cm^3]
18.3(12)	41.4(17)	97.3(70)	379(23)	516(32)

The second series of experiments were aimed at the proof of concept of the applicability of the diffusion model for temperature correction of the monitors

with passive sampling. These experiments were also aimed at the additional validation of the diffusion model. In these experiments the PIPS-system was connected to the exposure setup as it is shown in Figure 3. The exposure setup was used to ensure known activity concentration in the lower chamber of the PIPS-system. The PIPS-system was consecutively loaded with the studied membranes and the PIPS-detector was used to measure the activity concentration of radon/thoron in the upper chamber, which has penetrated through the membrane. In all experiments with radon, an exponentially decreasing activity concentration was used – in the beginning of the exposure the radon activity from the source was promptly introduced in the system, then the source was closed with valves and bypassed with an additional hose (not shown in Figure 3). The thoron exposures were carried out at constant thoron activity concentration.

A calibration of the PIPS-system for radon and thoron measurements was conducted. In these experiments the two chambers of the PIPS-system were separated by two mixed cellulose ester membrane filters (Millipore PHWP04700) with 0.3 μm pore size and thickness of about 150 μm each. These filters were chosen as they are transparent to both radon and thoron, efficiently stop their SDPs and are shown to be suitable for precise thoron penetration measurements (Mitev et al., 2020). For the calibration experiments pure radon or thoron atmosphere was created and the activity concentration was monitored by the AlphaGUARD. The alpha-spectra from the PIPS-detector were acquired and processed with the nanoMCA and the labZY software.

Once the system was calibrated, LDPE foils of different thicknesses (the same as those used for the diffusion chambers packing) were studied at different temperatures. For that purpose a LDPE foil of a given thickness was loaded in the PIPS-system in addition to the two cellulose filters used in the calibration. The temperatures of the air-conditioner and the thermostat were set to 16°C and when temperature equilibrium was reached the radon activity was promptly introduced in the experimental setup. The AlphaGUARD and the PIPS-detector followed the activity concentration in the lower and in the upper

chamber, respectively, until equilibrium is reached. Indication for that was the same rate of decrease of the two activity concentrations, see Eq. 10b. Then, the temperature was set to 21°C and some additional activity was promptly added and the same procedure was followed at that temperature. After that the same was repeated for 26°C. The additional input of activity between each exposure at different temperature was necessary because the radon activity concentration in the system was decreasing (due to decay and some leakage) while reaching equilibrium (up to 3-4 days). This procedure was followed for the studies of all foils.

Additionally, only the "18 μm" LDPE foil was studied at 21°C with thoron as the modeling showed that less than one percent of thoron would penetrate in the upper chamber even with the thinnest foil available. The equilibrium with thoron was reached fast (in less than 10 minutes due to its short half-life), however the experiment continued a few days in order to get better counting statistic.

4. Results and Discussion

After the exposure and the degassing of the diffusion chambers, their SSNTDs were etched to reveal the tracks and the tracks were counted visually with an optical microscope. Unexposed SSNTDs were also processed for background estimation. The track density n for each detector was estimated as the ratio $n = N/A$ of the number of the counted tracks N and the observed area A. Then, the net track density n_0 for each SSNTD was estimated as the difference $n_0 = n_s - n_b$ between the track density n_s of the exposed SSNTD and the background track density n_b. For all diffusion chambers the relative uncertainty of the track density was less than 5%. For each exposure the average net track density (hereafter the signal) of each couple of diffusion chambers (packed in foils of the same thickness or exposed bare) was estimated and is shown in Table 2. The ratios $n_{0,d_i} : n_{0,bare}$ of the signals of the packed n_{0,d_i} and the bare $n_{0,bare}$ chambers for each temperature were also estimated and is shown

in Table 2. The signal of the bare chambers is proportional to the activity concentration in the exposure media C_{out}, while the signal of the packed chambers is proportional to the activity concentration inside the given packaging $C_{in}(d,T)$. Thus, to validate the diffusion model the experimentally estimated ratios $n_{0,d_i} : n_{0,bare}$ were compared with the model-estimated ratios C_{in}/C_{out} (Eq. 14). The comparison is shown in Figure 4. As can be seen from Eq. 14 for fixed S/V of the packing, the studied ratio is a function of the thickness d and the permeability $P(T)$ of the packing. However, the temperature seems more intuitive and convenient parameter than the permeability and therefore in Figure 4 the temperature is used. In Figure 4(a) the studied ratios are presented as a function of the LDPE thickness for the three exposure temperatures and in Figure 4(b) the studied ratios are given as a function of the temperature for the three LDPE thicknesses. As can be seen there is a good agreement between the model and the experimental data within the uncertainties. This leads to the conclusion that the diffusion model describes well the behavior of diffusion chamber packed in anti-thoron packaging and proves the feasibility of the optimization approach described in Section 2.2. This also allows to speculate that foils of the same producer's batch (even with different thicknesses) posses similar diffusion properties (permeabilities).

The results from these experiments were also used to check the applicability of the differential method described in Section 2.2. For that purpose the ratios R_s was experimentally estimated as $R_s(d_1,d_2;T) = n_{0,d_1} : n_{0,d_2}$, (shown in Table 2). In Figure 5 these ratios are plotted versus the exposure temperature and compared with the model estimated dependence $R_s(d_1,d_2;T)$ (Eq 17) using the already known $P(T)$-dependence (Georgiev et al., 2019). The results in the figure confirm that the packagings with bigger difference in the thicknesses ensure better temperature sensitivity of $R_s(T)$ in agreement with what was noted in Section 2.2. Figure 5 shows how the exposure temperature could be estimated. This temperature could be used to estimate the ratio C_{in}/C_{out} for the given packing thickness (e.g. see Figure 4(b)) which actually accounts for the temperature bias of the packed passive devices. This approach was applied

Table 2: For each exposure temperature are given: The average net track density ($n_{0,bare}$, n_{0,d_i}) of diffusion chambers packed in foils of the same thickness or exposed bare; The ratios ($n_{0,d_i} : n_{0,bare}$) of the net track densities of the packed and the bare chambers; The ratios ($n_{0,d_i} : n_{0,d_j}$) of the net track densities of chambers with different packaging. The uncertainties are at the level of 1σ.

	Packaging thickness			
	bare	18μm	41μm	97μm
T[°C]	$n_{0,bare}$ [cm^{-2}]	$n_{0,18}$ [cm^{-2}]	$n_{0,41}$ [cm^{-2}]	$n_{0,97}$ [cm^{-2}]
10(1)	7160(260)	6430(260)	5800(240)	4380(180)
20(1)	6360(240)	6100(240)	5480(220)	4960(250)
30(1)	4440(190)	4400(200)	4280(180)	3870(180)
T[°C]		$n_{0,d_i} : n_{0,bare}$		
10(1)	1	0.899(48)	0.810(44)	0.612(34)
20(1)	1	0.960(53)	0.861(48)	0.779(50)
30(1)	1	0.992(62)	0.964(59)	0.873(57)
T[°C]		$n_{0,97} : n_{0,18}$	$n_{0,41} : n_{0,18}$	$n_{0,97} : n_{0,41}$
10(1)		0.681(39)	0.901(51)	0.756(44)
20(1)		0.812(52)	0.897(51)	0.905(59)
30(1)		0.880(58)	0.972(60)	0.905(58)

to the signal of the chambers shown in Table 2 and the results are given in Table 3. The ratios $R_s(d_1 = 97\ \mu m, d_2 = 18\ \mu m; T)$ were used to estimate the temperature T_{est} in the three exposures. The estimated temperatures were used to estimate $\kappa_{d_i}(T_{est}) = C_{in}/C_{out}$ similarly to the curves plotted in Figure 4(b). The corrected signal was estimated as $n_{\kappa,d_i} = n_{0,d_i}/\kappa_{d_i}$ (Table 3). Although the temperature estimation is not very good, a very good agreement between the corrected signal of the packed chambers and the bare chambers is observed. Moreover, the uncertainty of the signal of the chambers packed in thinner foil is barely increased. This is due to the fact that the correction coefficient $\kappa =$

C_{in}/C_{out} and the ratio R_s are correlated (see Eq. 19) and the intermediate poor estimation of the temperature does not affect the correct estimation of $\kappa(R_s)$. Additionally, for thin foil κ is close to 1 and changes slightly with the temperature, and therefore the uncertainty of the temperature does not contribute significantly to the uncertainty of κ. These observations are also confirmed by Figure 6 (described in the next paragraph).

Table 3: Demonstration of the differential method (Section 2.2): The experimentally estimated ratios $n_{0,97} : n_{0,18}$ (from Table 2) are used to estimate the exposure temperature T_{est}. This temperature is used to calculate κ_{d_i} by the model. The net track densities of the packed diffusion chambers (from Table 2) are corrected $n_{\kappa,d_i} = n_{0,d_i}/\kappa_{d_i}$ and are compared with $n_{0,bare}$. The uncertainties are at the level of 1σ.

$n_{0,97} : n_{0,18}$	T_{est}[°C]	κ_{18}	κ_{41}	κ_{97}
0.681(39)	9(3)	0.90(3)	0.79(4)	0.62(6)
0.812(52)	18(5)	0.95(2)	0.89(4)	0.77(6)
0.880(58)	25(6)	0.97(2)	0.93(4)	0.86(7)
T_{est}[°C]	$n_{0,bare}$ [cm^{-2}] (to compare with)	$n_{\kappa,18}$ [cm^{-2}]	$n_{\kappa,41}$ [cm^{-2}]	$n_{\kappa,97}$ [cm^{-2}]
9(3)	7160(260)	7150(370)	7340(480)	7070(750)
18(5)	6360(240)	6430(290)	6150(370)	6440(600)
25(6)	4440(190)	4540(230)	4600(280)	4500(430)

The other way to apply the diffusion method is the direct experimental estimation of $CF_i(R_s)$ and $\kappa_i(R_s)$ during the calibration of the device couples. However, it is still based on the model: it is known that the dependence $\kappa_i(R_s(T))$ exists and it applies to the calibration factors of the devices from the couple as $CF_i = CF\kappa_i$. The device couple could be calibrated in their packagings at a few different values of R_s (e.g. at different temperatures) and thus, the $CF_i(R_s)$ dependence could be estimated experimentally. Then in the field measurements of radon, the ratio $R_s(d_1, d_2; T) = n_{0,d_1} : n_{0,d_2}$ could be measured experimentally and the calibration factor could be determined directly

from $CF_i(R_s)$. An example for that application is given in Figure 6. For that example the modeled dependence $\kappa_i(R_s(T))$ for the diffusion chambers packed in 18 μm and 97 μm foils is assumed to be the calibration-estimated dependence. The experimentally obtained ratio R_s(97 μm,18 μm;T)= $n_{0,97} : n_{0,18}$ (shown in Table 2) presented in the figure as black dashed line is used to estimate (dashed arrows) the corresponding "calibration factors" (κ_i in this example). For the comparison purposes the ratios $n_{0,d_i} : n_{0,bare}$ (see Table 2) that should correspond to the "true" values of κ_i are shown as dots. The very good agreement observed in Figure 6 proves the applicability of the differential method for temperature correction of the radon measurements with passive devices packed in anti-thoron membranes.

The second series of experiments were dedicated to monitors with passive sampling and for that purpose the upper chamber of the PIPS-system (see Figure 3) was considered to be such a monitor. The PIPS-system was calibrated for radon and thoron measurement as described in Section 3. In Figure 7 examples of the obtained alpha-spectra of radon and thoron with their SDPs are shown. It is seen that in the case of pure radon or thoron atmosphere the alpha-peaks of the radon SDPs – ^{218}Po (6.00 MeV, $T_{1/2}$=3.071(22) min (Bé et al., 2016)) and ^{214}Po (7.69 MeV, $T_{1/2}$=0.1623(12) ms (Bé et al., 2016)) and the thoron SDP – ^{216}Po (6.78 MeV, $T_{1/2}$=0.148(4) s (Bé et al., 2016)) are well separated, which makes them suitable for measurements and therefore these peaks (nuclides) were used for the calibration. A drawback of ^{214}Po is that it is preceded in the decay chain of radon by ^{218}Po, ^{214}Pb ($T_{1/2}$=26.916(44) min (Bé et al., 2016)) and ^{214}Bi ($T_{1/2}$=19.8(1) min (Bé et al., 2016)) and, in order to be used for measurement and calibration, at least 3 hours are needed to reach secular equilibrium. However, in case of mixed radon-thoron atmosphere ^{214}Po is more suitable for radon measurement as the ^{218}Po peak overlaps with the alpha-peaks of thoron SDPs, see Figure 7(b).

In the calibration procedures with radon or thoron at least 10 equilibrium spectra were obtained with counting statistics in Region of Interest (ROI) of each calibration alpha-peak better than 1.5%. The counting rate ν in each peak

was estimated as the ratio $\nu = \Sigma/t_l$ between the total counts Σ in the ROI of the alpha-peak (see the peak-marking in Figure 7(b)) and the live time t_l for the spectra acquisition. Background measurements were also carried out and the background counting rate in each alpha-peak ROI was found to be below 0.1% of the counting rate during the calibration. The net counting rate ν_0 was estimated as the difference $\nu_0 = \nu_s - \nu_b$ between the counting rates in the given alpha-peak ROI in the calibration spectrum ν_s and the background spectrum ν_b. Two efficiencies for each nuclide were estimated: 1. The "volumic" efficiency $\epsilon_{v,i}$ was estimated as the ratio $\epsilon_{v,i} = \nu_{0,i}/C_{cal}$ of the net counting rate in the given alpha-peak and the activity concentration C_{cal} of radon or thoron measured by the AlphaGUARD, and 2. The efficiency ϵ_i was estimated as the product $\epsilon_i = \epsilon_{v,i}V$ of the "volumic" efficiency and the volume V=15.64(18) cm^3 of the upper chamber. The volumic efficiency $\epsilon_{v,i}$ is more convenient to work with as it allows to estimate directly the activity concentration in the upper chamber, while the efficiency ϵ_i gives information about the particles detected per one decay of radon or thoron. The obtained efficiencies were averaged over all calibration spectra used and the average values are shown in Table 4.

Table 4: Efficiencies and volumic efficiencies of the PIPS-system for the radon SDPs – ^{218}Po and ^{214}Po and the thoron SDP – ^{216}Po. The uncertainties of the obtained efficiencies are given at the level of 1σ. The alpha-particles energies E are also given according to Bé et al. (2016).

Nuclide	E_α [keV]	ϵ_v [10^{-6}m^{-3}]	ϵ
^{218}Po (radon)	6002.35(9)	6.80(37)	0.435(23)
^{214}Po (radon)	7686.82(6)	6.71(37)	0.429(24)
^{216}Po (thoron)	6778.4(5)	5.08(54)	0.325(35)

The next experiments were carried out with LDPE membranes of different thickness separating the two chambers of the PIPS system as described in Section 3. The purpose was to check the applicability of the diffusion model for temperature correction of the readings of monitors with passive sampling

and to validate additionally the diffusion model with a different experimental setup. The activity concentrations in the lower and in the upper chambers of the PIPS system were continuously measured by the AlphaGUARD and the PIPS-detector, respectively. When an equilibrium was reached, the obtained activity concentrations were used to estimate the ratio C_{in}/C_{out} (i.e. the PIPS-system signal over the AlphaGUARD signal) and it was compared with the model expectation (shown in Figure 8). During the experiment a small activity leakage was observed in the upper detector chamber. To account for such leakage the decay constant λ of radon in Eq. 5 (which accounts for the decay/decrease of radon in the detector's chamber) was replaced by an effective decrease constant λ_{eff} which accounts for both decay and leakage. This lead to the replacement of λ with λ_{eff} in the solutions of Eq. 5. For instance, Eq. 10a takes the form:

$$C_{in}(t) = \frac{C_{out}(t)}{(1 + \frac{\lambda_{eff}}{\lambda_d})}\left(1 - e^{(-(\lambda_{eff}+\lambda_d)t)}\right) \tag{20}$$

In the present experiments this constant was estimated to be λ_{eff} ≈0.0135h $^{-1}$. In Figure 8(a) the effect of λ_{eff} is demonstrated: the dashed line represents the modeled ratio C_{in}/C_{out} if there was no leakage and C_{in} decreases only due to radon decays (i.e. λ_{eff}=λ_{radon} ≈0.0076h $^{-1}$) and the solid line is the modeled ratio C_{in}/C_{out} with the estimated λ_{eff} ≈0.0135h $^{-1}$. The dots represent the experimental ratio for the LDPE foil of 91.2(13) μm the permeability of which is known (the permeability of this foil is studied in (Georgiev et al., 2019)). As it is seen there is an excellent agreement between the diffusion model and the experimental results. The comparison for the three foils with the diffusion model (with the leakage taken into account) are shown in Figure 8(b). A good agreement is also observed for the 18.4 μm foil, however the 39.4 μm foil shows slight discrepancies. It was assumed earlier that the foils of the same batch should have the same permeability and this was supported by the diffusion chambers results. However, the results with the PIPS system indicated that such assumption could be incorrect. Therefore, it is highly recommended to characterize each membrane in terms of permeability before its usage as a diffusion barrier.

Figure 9 shows the temperature and the activity concentration measured by the AlphaGUARD and the activity concentration measured by the PIPS system during the study of the 91.2(13) μm membrane. When the temperature is changed, an activity is added to the system and the equilibrium is broken. After a while an equilibrium is reached again and an indication for that is the same slope of C_{in} and C_{out}, however they differ due to the diffusion resistivity introduced by the membrane. As the diffusion properties (i.e. the permeability) of the membrane is known, the diffusion model and the temperature data were used and readings of the PIPS system were corrected ($C_{in,corr}$) to account for the diffusion resistivity of the membrane at the given temperature. The very good agreement between $C_{in,corr}$ and C_{out} when equilibrium is reached shows that the proposed approach could be applied for monitors with passive sampling protected with anti-thoron membrane. It is also seen from the figure that if a membrane is used for anti-thoron protection, it introduces a time delay which could be significant if the diffusion parameters of the membrane are not chosen properly. This points out again that the diffusion properties of the membranes should be studied prior their usage as thoron barriers.

In the last experiment the same setup was used with the thoron source. The preliminary estimation by the model showed that if the thinnest foil (18.4(11) μm) is used and the temperature is set to 21°C the equilibrium ratio should be $C_{in}/C_{out} \approx 0.4(1)\%$. Such low penetration ratio is very sensitive to the experimental conditions and the diffusion properties of the membrane, which were actually transferred from the 91.2 μm as already noted. However, the experimentally estimated ratio of 0.6(1)% was in good agreement with the model expectation, considering the low activity (about 0.03 Bq) in the upper chamber that was measured in order to estimate the ratio. Thus, the model seems also applicable for studies of thoron transport.

The results of this study also indicate that the PIPS system can be applied very well for continuous monitoring of the changes of radon and thoron concentrations during calibrations and measurements. Thus, the system appears to be a valuable tool in the characterization of the timing response of active radon

monitors.

5. Conclusions

A verified model (Mosley, 1996) of the diffusion of radon through a membrane in a defined volume was modified and further developed to allow modeling the effect of anti-thoron membranes on the response of radon detectors to radon and thoron. The model is validated and three approaches are proposed that allow to use diffusion membranes with known diffusion properties to improve the performance of radon detectors.

The first approach allows to model and estimate the thoron reduction and the temperature bias which is introduced by a membrane with known diffusion properties if it is used as a packaging of a passive radon device. The approach allows to optimize the packaging to obtain reasonable reduction of the thoron influence while minimizing the temperature bias. It is shown that the thoron influence could be lowered to less than 2% (in terms of percentage of thoron that penetrates the packaging) with temperature bias within 2% considering calibration at 20°C with temperature values within 10-30°C.

The second approach (the differential method) uses a couple of passive devices packed in two packages with different diffusion properties. The ratio of the signal of the two devices is temperature dependent. Thus, this ratio could be used to deduce and account for the temperature bias. The applicability of the differential method is demonstrated and conclusions are drawn considering the optimal choice of the packings of the two detectors in the couple.

The third approach is applicable to radon monitors with passive sampling protected with anti-thoron membrane. The idea is to use the temperature measurements of the monitor (currently most radon monitors measure the temperature), the already known diffusion properties of the membrane and the diffusion model to calculate and apply on-line temperature correction of the measurements of the monitor. The applicability of the approach is demonstrated. A potential drawback of this approach is the time-delay of the response of the de-

tector due to the diffusion resistivity of the membrane. Therefore, the approach cannot be directly applied if a fast response of the monitor is required. It is speculated that a possible solution could be found if the differential signal of the detector (the difference between two consecutive measurements related to the time between them) is used in combination of the diffusion model to recover rapid changes. However, a dedicated study is required to study this opportunity.

In the course of this work, the PIPS system used in the studies was found to be very appropriate for study of the permeability of thin membranes. The system is almost the same as the French (CEA/LNHB) reference thoron detector and allows precise measurement of the activity penetrating the membrane, which is of high importance for the permeability estimation. It also allows precise studies of the diffusion dynamics including at non-constant temperature. A small drawback is that the PIPS system is applicable only for thin membranes with thickness much smaller than the diffusion length of radon in the membrane, which is fulfilled for the anti-thoron membranes. Additionally, the PIPS system is found to be a very useful tool for characterization of the timing response of active radon monitors.

Acknowledgment

This research is funded in part by the Bulgarian National Science Fund under project SPIRAD, contact KP-06-H48/3 from 26.11.2020.

This research is funded in part by the European Metrology Programme for Innovation and Research (EMPIR), JRP-Contract 16ENV10 MetroRADON (www.euramet.org). The EMPIR initiative is co-funded by the European Union's Horizon 2020 research and innovation progamme and the EMPIR Participating States.

The authors are indebted to Ivelina Dimitrova PhD for reading and commenting the manuscript.

References

Azimi-Garakami, D., Flores, B., Piermattei, S., Susanna, A.F., Seidel, J.L., Tommasino, L., Torri, G., 1988. Radon gas samplers for indoor and soil measurements and its applications. Radiation Protection Dosimetry 24, 269–272. doi:10.1093/oxfordjournals.rpd.a080284.

Bé, M.M., Chisté, V., Dulieu, C., Kellett, M., Mougeot, X., Arinc, A., Chechev, V., Kuzmenko, N., Kibédi, T., Luca, A., Nichols, A., 2016. Monographie BIPM-5: Table of Radionucleides. volume 8. Bureau International des Poids et Mesures, France. URL: http://www.bipm.org/utils/common/pdf/monographieRI/Monographie_BIPM-5_Tables_Vol8.pdf. ISBN-13: 978-92-822-2264-5 .

Bochicchio, F., Ampollini, M., Tommasino, L., Sorimachi, A., Tokonami, S., 2009. Sensitivity to thoron of an SSNTD-based passive radon measuring device: Experimental evaluation and implications for radon concentration measurements and risk assessment. Radiation Measurements 44, 1024–1027. doi:10.1016/j.radmeas.2009.10.090.

Chen, J., Moir, D., 2012. A study on the thoron sensitivity of radon detectors available to canadians. Journal of Radiological Protection 32, 419–425. doi:10.1088/0952-4746/32/4/419.

De Simone, G., Lucchetti, C., Galli, G., Tuccimei, P., 2016. Correcting for H_2O interference using a RAD7 electrostatic collection based silicon detector. Journal of Environmental Radioactivity 162-163 (2016) 146e153 162–163, 146–153. doi:10.1016/j.jenvrad.2016.05.021.

Dwivedi, K., Mishra, R., Tripathy, S., Kulshreshtha, A., Sinha, D., Srivastava, A., Deka, P., Bhattacharjee, B., Ramachandran, T., Nambi, K., 2001. Simultaneous determination of radon, thoron and their progeny in dwellings. Radiation Measurements 33, 7–11. doi:10.1016/S1350-4487(00)00131-1.

Fleischer, R.L., Giard, W.R., Mogro-Campero, A., Turner, L.G., Alter, H.W., Gingrich, J.E., 1980. Dosimetry of environmental radon: Methods and theory for low-dose integrated measurements. Health Physics 39, 957–962. doi:10.1097/00004032-198012000-00009.

Fleischer, R.L., Giard, W.R., Turner, L.G., 2000. Membrane-based thermal effects in ^{222}Rn dosimetry. Radiation Measurements 32, 325–328. doi:10.1016/S1350-4487(00)00046-9.

Galli, G., Cannelli, V., Nardi, A., Piersanti, A., 2019. Implementing soil radon detectors for long term continuous monitoring. Applied Radiation and Isotopes 153, 108813. doi:1016/j.apradiso.2019.108813.

Georgiev, S., Mitev, K., Dutsov, C., Boshkova, T., Dimitrova, I., 2019. Partition coefficients and diffusion lengths of ^{222}Rn in some polymers at different temperatures. International Journal of Environmental Research and Public Health 16, 4523. doi:10.3390/ijerph16224523.

Ggriffith, R.V., Tommasino, L., 1990. Etch track detectors in radiation dosimetry, in: Kase, K.R., Bjärngard, B.E., Attix, F.H. (Eds.), The Dosimetry of Ionizing Radiation. Academic Press, San Diego. chapter 4, pp. 323 – 426. doi:10.1016/B978-0-12-400403-0.50008-7.

Hafez, A., Somogyi, G., 1986. Determination of radon and thoron permeability through some plastics by track technique. International Journal of Radiation Applications and Instrumentation. Part D. Nuclear Tracks and Radiation Measurements 12, 697–700. doi:10.1016/1359-0189(86)90682-5.

Hopper, R.D., Steinhäusler, F., Ronca-Battista, M., 1999. Iaea/epa international climatic test program for integrating radon detectors. Health Physics 77, 303–308. doi:10.1097/00004032-199909000-00009.

Mark Baskaran, 2016. Radon: A Tracer for Geological, Geophysical and Geochemical Studies. Springer International Publishing AG, Switzerland. doi:10.1007/978-3-319-21329-3.

Meisenberg, O., Mishra, R., Joshi, M., Gierl, S., Rout, R., Lu Guo, Agarwal, T., Kanse, S., Irlinger, J., Sapra, B.K., Tschiersch, J., 2017. Radon and thoron inhalation doses in dwellings with earthen architecture: Comparison of measurement methods. Science of the Total Environment 579, 1855–1862. doi:10.1016/j.scitotenv.2016.11.170.

Michielsen, N., Bondiguel, S., 2015. The influence of thoron on instruments measuring radon activity concentration. Radiation Protection Dosimetry 167, 289–292. doi:10.1093/rpd/ncv264.

Miles, J., Ibrahimi, F., Birch, K., 2009. Moisture-resistant passive radon detectors. Journal of Radiological Protection 29, 269–271. doi:10.1088/0952-4746/29/2/N01.

Mitev, K., Cassette, P., Pressyanov, D., Georgiev, S., Dutsov, C., Michielsen, N., Sabot, B., 2020. Methods for the experimental study of ^{220}Rn homogeneity in calibration chambers. Applied Radiation and Isotopes , 109259doi:10.1016/j.apradiso.2020.109259.

Mosley, R., 1996. Description of a method for measuring the diffusion coefficient of thin films to ^{222}Rn using a total alpha detector, in: 1996 International Radon Symposium, Haines City, FL, USA.

Nikolaev, V., Ilić, R., 1999. Etched track radiometers in radon measurements: a review. Radiation Measurements 30, 1–13. doi:10.1016/S1350-4487(98)00086-9.

Papastefanou, C., 2002. An overview of instrumentantion for measuring radon in soil gas and groundwaters. Journal of Environmental Radioactivity 63, 271–283. doi:10.1016/S0265-931X(02)00034-6.

Pressyanov, D., Mitev, K., Georgiev, S., Dimitrova, I., Kolev, J., 2017. Laboratory facility to create reference radon + thoron atmosphere under dynamic exposure conditions. Journal of Environmental Radioactivity 166, 181–187. doi:10.1016/j.jenvrad.2016.03.018.

Sabot, B., 2015. Calibration of thoron activity concentration monitors. Ph.D. thesis. Gif-sur-Yvette, France. URL: https://tel.archives-ouvertes.fr/tel-01253649.

Sabot, B., Pierre, S., Michielsen, N., Bondiguel, S., Cassette, P., 2016. A new thoron atmosphere reference measurement system. Applied Radiation and Isotopes 109, 205–209. doi:10.1016/j.apradiso.2015.11.055.

Tokonami, S., Yang, M., Sanada, T., 2001. Contribution from thoron on the response of passive radon detectors. Health Physics 80, 612–615. doi:10.1097/00004032-200106000-00014.

Tommasino, L., 1990. Radon monitoring by alpha track detection. International Journal of Radiation Applications and Instrumentation. Part D. Nuclear Tracks and Radiation Measurements 17, 43 – 48. doi:10.1016/1359-0189(90)90147-P.

Tommasino, L., 1998. Passive sampling and monitoring of radon and other gases. Radiation Protection Dosimetry 78, 55 – 58. doi:10.1093/oxfordjournals.rpd.a032333.

UNSCEAR, 2000. Sources and Effects of Ionizing Radiation. UNSCEAR 2000 Report to the General Assembly, with Scientific Annexes: Annex B. United Nations, New York, USA.

UNSCEAR, 2008. Sources and Effects of Ionizing Radiation. UNSCEAR 2006 Report to the General Assembly, with Scientific Annexes: Annex E. United Nations, New York, USA.

Ward III, W.J., Fleischer, R.L., Mogro-Campero, A., 1977. Barrier technique for separate measurement of radon isotopes. Review of Scientific Instruments 48, 1440–1441. doi:10.1063/1.1134915.

WHO, 2009. WHO Handbook on Indoor Radon: A Public Health Perspective. World Health Organization. URL:

https://www.who.int/ionizing_radiation/env/9789241547673/en/.
ISBN-13: 978-92-4-154767-3 .

Figure captions

Fig. 1. Scheme of the experimental setup used by Mosley (1996). It consist of a source chamber in which the radon concentration C_{out} is kept constant, an accumulation chamber with defined volume V and an alpha-detector inside (not shown) and a film with defined thickness d and surface S the diffusion properties of which are to be studied.

Fig. 2. Example for the thoron and the temperature influence on the radon signal of a passive device introduced by its LDPE package estimated by the diffusion model. The curves represent the percentage of thoron from the ambient media that penetrates inside the packing. The straight lines represent the relative temperature bias in the radon penetration inside the packaging of the passive device if the device is calibrated for radon measurements at 20°C.

Fig. 3. Scheme of the experimental setup. The right-side part is an enlarged scheme of the PIPS-system used to study the response of monitors with passive sampling protected by a polymer (LDPE) membrane. The left-side part is the Exposure setup used: 1. To create known radon/thoron activity concentration for the studies with the PIPS-system and 2. To expose the passive devices (in this case the PIPS-system was disconnected). Each element of the experimental setup has a couple of valves (not shown) that allows the element to be isolated without activity loss.

Fig. 4. Comparison of the experimental data for $n_{0,d_i} : n_{0,bare}$ obtained with the diffusion chambers (dots), shown in Table 2 and the diffusion model estimated ratio C_{in}/C_{out} (solid lines), estimated by Eq. 14. In (a) these ratios are given as a function of the packaging thickness for the three exposure temperatures and in (b) the ratios are given as a function of the exposure temperature for the three packaging thicknesses. The dashed lines mark the 1σ uncertainty range of the corresponding solid lines, that is due to the uncertainty of the permeability. The uncertainties of the experimental points are about 5–6% at the level of 1σ for all points (not shown).

Fig. 5. Comparison of the experimental results (dots) and model estimated

(solid lines) dependence $R_s(d_1, d_2; T) = n_{0,d_1} : n_{0,d_2}$ for three cases of device couple packing. The case with the biggest difference in the packaging thicknesses is used to demonstrate (dashed arrow) the estimation of the exposure temperature.

Fig. 6. Comparison of the experimental results (dots) and model estimated (solid lines) dependence $\kappa_i(R_s)$ for the two devices of the device couple packed in LDPE membranes with d_1=97 μm and d_2=18 μm. It is also demonstrated (dashed arrows) how the experimental value of $R_{s,exp}$ could be used to estimate the value of $\kappa_i(R_{s,exp})$ from the "calibration dependences". The uncertainties of the experimental points are about 5–7% at the level of 1σ for all points (not shown).

Fig. 7. (a) A screenshot of a radon spectrum acquired with the labZY software in a single measurement with the PIPS system. The alpha-peaks of ^{218}Po (6.00 MeV) and ^{214}Po (7.69 MeV) are marked. (b) Several radon and thoron spectra, acquired in the same way, are summed for better visualization of all alpha-peaks in radon and thoron chains. The alpha-particles of radon and thoron form continuum as their atoms are not charged and they are spread in the volume of the chamber. On the other hand, the decay products are charged and therefore captured at the PIPS surface by the HV applied (see Figure 3) and form narrow, well resolved peaks. Due to the very small half-life of ^{212}Po (300(2) ns (Bé et al., 2016)), its alpha-particles are registered in coincidence with the beta-particles of its predecessor ^{212}Bi which results in a high-energy tailing of the ^{212}Po alpha-peak with the shape of ^{212}Bi beta-spectrum.

Fig. 8. Comparison between the experimentally obtained (dots) and the modeled (lines) ratio C_{in}/C_{out} as a function of the temperature for the LDPE foils with three thicknesses. During the experiments leakage was observed. In (a) the effect of the leakage is demonstrated for the 91.2 μm membrane – the dashed line is the model expectation without taking into account the leakage and for the solid line the leakage is taken into account. In (b) for all model-expectation curves the leakage is taken into account.

Fig. 9. Activity concentration and temperature follow-up during the ex-

periments with the 91.2 μm LDPE foil. It is seen that after equilibrium the activity concentrations in the ambient media measured by the AlphaGUARD (C_{out}) and in the upper chamber of the PIPS system (C_{in}) have the same slope but they differ. After taking into account the temperature (T°C) and using the model to estimate the temperature correction, the corrected activity concentrations in the upper chamber of the PIPS system ($C_{in,corr}$) coincides very well with the ambient concentration measured by the AlphaGUARD.

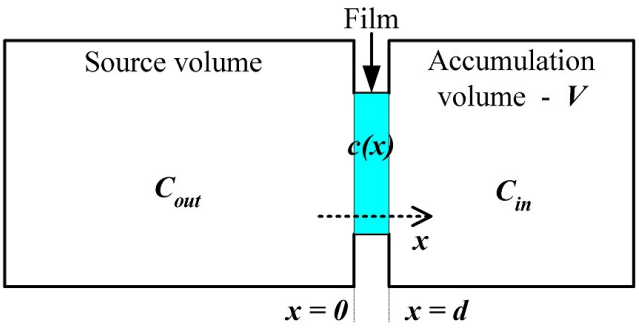

Figure 1:

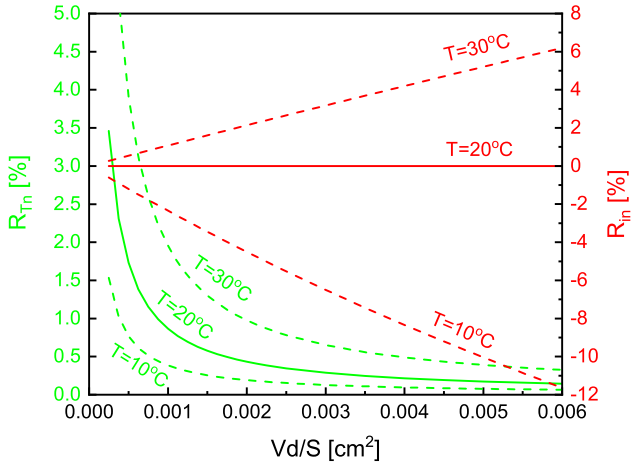

Figure 2:

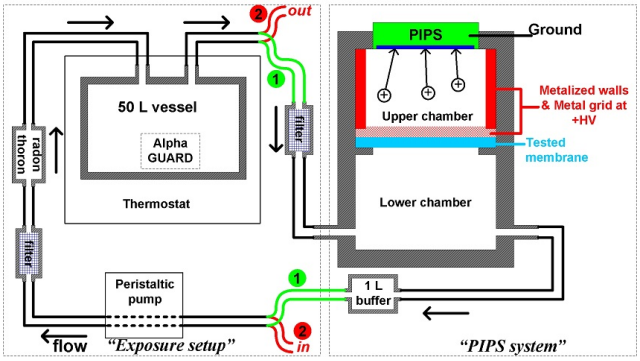

Figure 3:

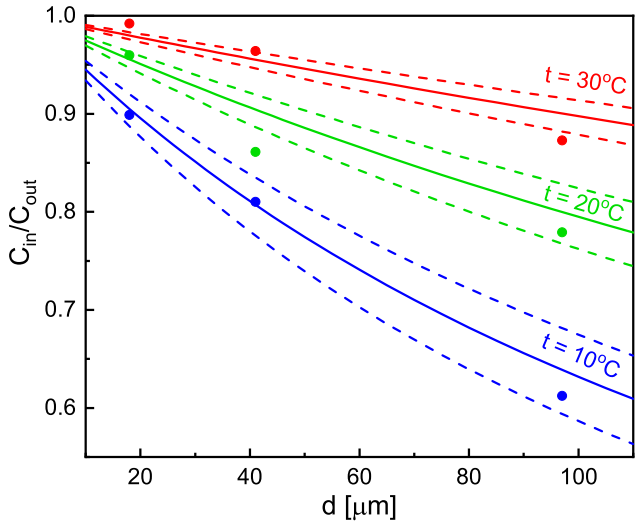
1.0
0.9
0.8
0.7
0.6
C_{in}/C_{out}
20
40
60
80
100
d [μm]
t = 30°C
t = 20°C
t = 10°C

(a)

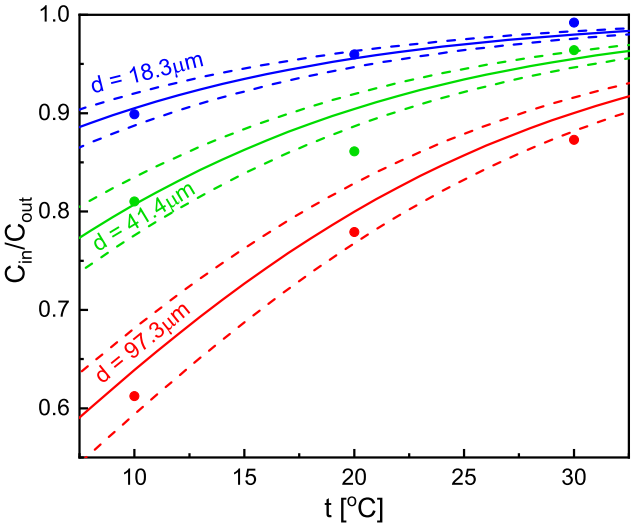
1.0
0.9
0.8
0.7
0.6
C_{in}/C_{out}
10
15
20
25
30
t [°C]
d = 18.3μm
d = 41.4μm
d = 97.3μm

(b)

Figure 4:

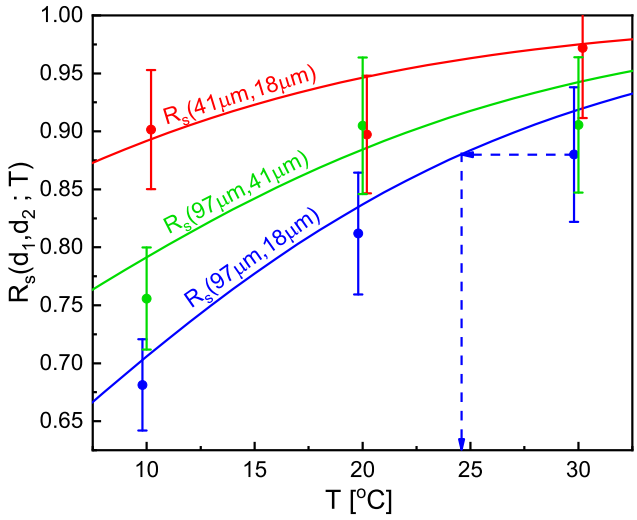

Figure 5:

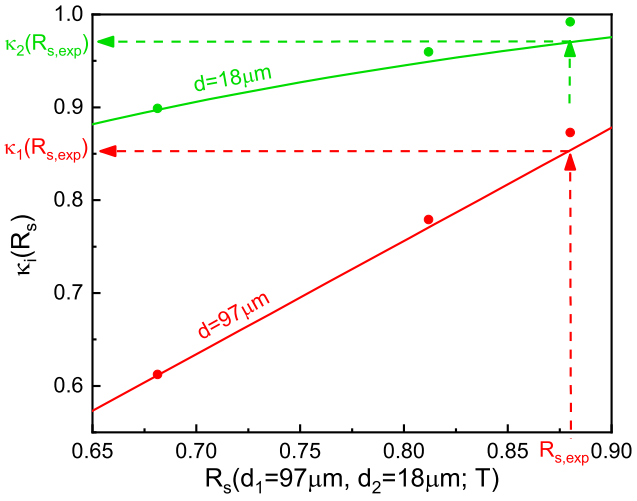

Figure 6:

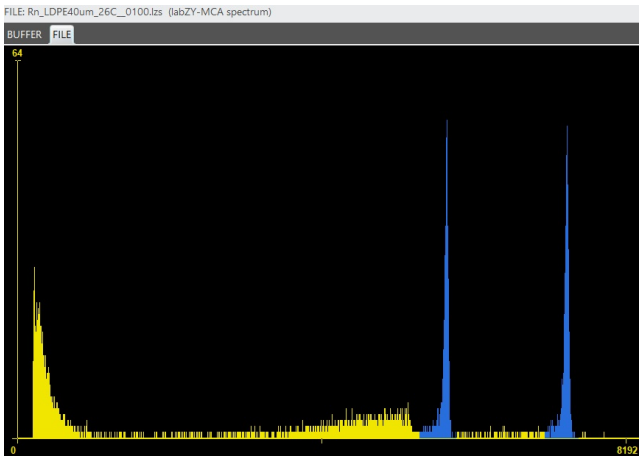
FILE: Rn_LDPE40um_26C__0100.lzs (labZY-MCA spectrum)
BUFFER
FILE
64
0
8192

(a)

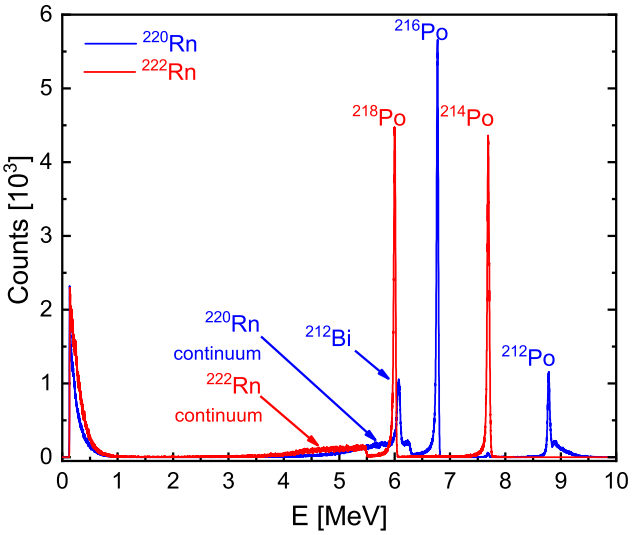
Counts [10^3]
E [MeV]
220Rn
222Rn
216Po
218Po
214Po
212Po
212Bi
220Rn
continuum
222Rn
continuum

(b)

Figure 7:

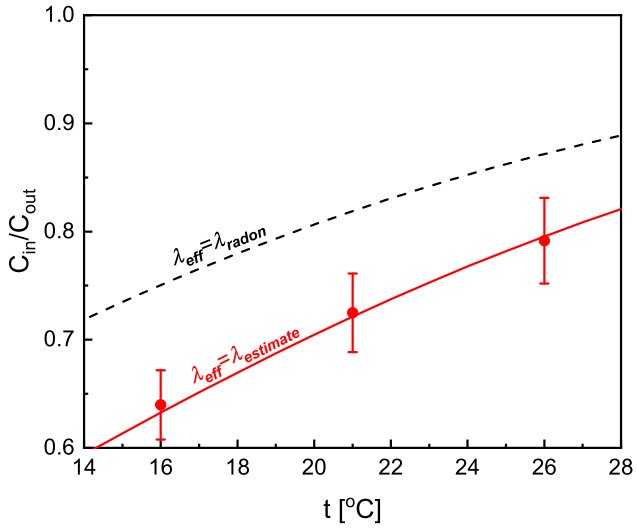
1.0
0.9
0.8
0.7
0.6
C_{in}/C_{out}
$\lambda_{eff}=\lambda_{radon}$
$\lambda_{eff}=\lambda_{estimate}$
14
16
18
20
22
24
26
28
t [°C]

(a)

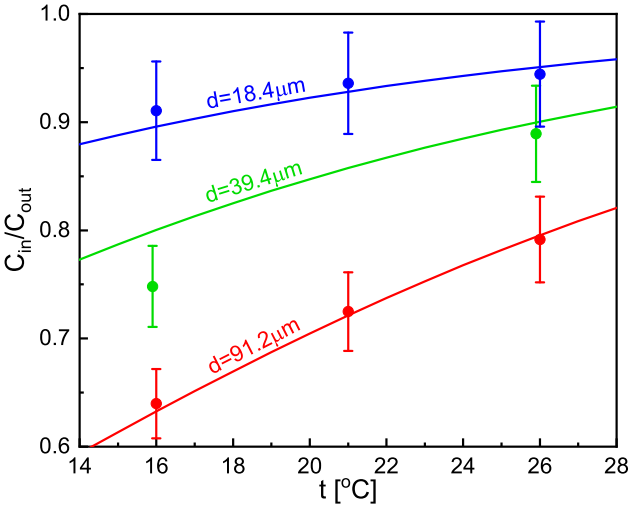
1.0
0.9
0.8
0.7
0.6
C_{in}/C_{out}
d=18.4μm
d=39.4μm
d=91.2μm
14
16
18
20
22
24
26
28
t [°C]

(b)

Figure 8:

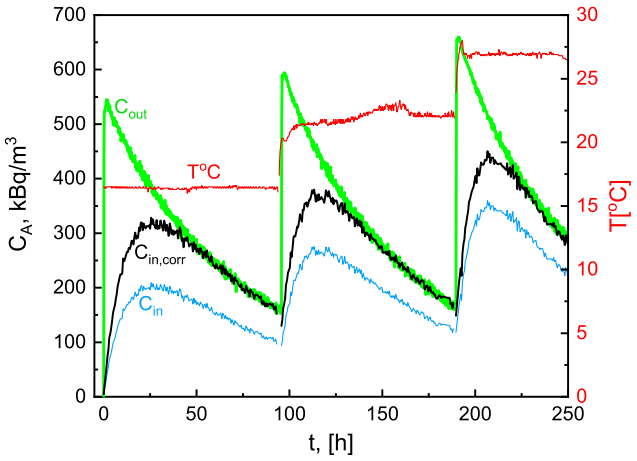
700
600
500
400
300
200
100
0
0
50
100
150
200
250
t, [h]
30
25
20
15
10
5
0
T[°C]
C_A, kBq/m^3
C_out
T°C
C_in,corr
C_in

Figure 9: